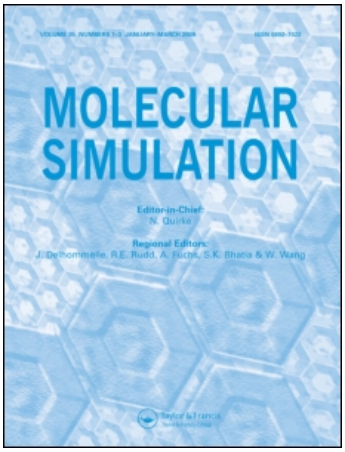

Molecular Simulation
Publication details, including instructions for authors and subscription information:
http://www.informaworld.com/smpp/title~content=t713644482

Molecular Dynamics Study of Nitrogen in Slit Micropores

P. Ravi[a]; S. Murad[a]
[a] Chemical Engineering Department, University of Illinois at Chicago, Chicago, Illinois, USA

To cite this Article Ravi, P. and Murad, S.(1993) 'Molecular Dynamics Study of Nitrogen in Slit Micropores', Molecular Simulation, 11: 2, 93 — 104
To link to this Article: DOI: 10.1080/08927029308022502
URL: http://dx.doi.org/10.1080/08927029308022502

Molecular Simulation, 1993, Vol. 11(2-4), pp. 93-104
Reprints available directly from the publisher
Photocopying permitted by license only

MOLECULAR DYNAMICS STUDY OF NITROGEN IN SLIT MICROPORES

P. RAVI and S. MURAD

Chemical Engineering Department, University of Illinois at Chicago, Chicago, Illinois 60680-4348 USA

(Received December 1992, accepted March 1993)

We present results of a computer simulation study of fluid nitrogen in model slit micropores. The model used for the micropore allows for the permeability of the pore wall to the confined fluid to be precisely controlled, while maintaining the atomic nature of the wall. Density and orientation profiles, wall permeabilities and diffusion coefficients have been obtained for systems with pore walls ranging from the almost impermeable to the completely permeable. Both the density and orientation profiles exhibit nonuniform behavior, while we observe anisotropy in the diffusion coefficients.

KEY WORDS: Micropores, slit pores, atomic walls, nitrogen, permeability, anisotropy

1 INTRODUCTION

Fluids in microporous materials, such as activated carbon, silica gel, porous rock, etc. exhibit unusual behavior such as nonuniform density distributions, phase transitions, preferential adsorption in mixtures, and many others [1-4]. An understanding of this behavior is important for many industrial processes, including, catalysis, tertiary oil recovery, chromatography, separation technologies - especially biological and biochemical [5], etc. Although, traditionally, macroscopic (continuum) hydrodynamics has been used to study and characterize fluids in these systems, it has not been very successful because of the inherent microscopic nature of these porous materials. In most cases the structure of the porous material (pore size, pore shape, interconnectivity, etc.) is poorly characterized [2, 4]. The pore size in these systems typically ranges from 20 to 30 Å [1, 2, 4]. This small size leads to strong interactions between the fluid and pore particles, leading to the unusual behavior of the fluid. Experimental studies of these systems is difficult at the molecular level, as evidenced by the rather small number reported in the literature [6-9]. However computer simulation methods and molecular theories can be used to develop an understanding of fluid behavior in these confined systems, and help in the design of such systems for specific industrial applications.

Most of the studies reported in the literature on fluids in microporous systems have been for monatomic fluids in impermeable model pores, although there have been a few studies on polyatomic fluids in confined systems [10-14]. Here we report a study of fluid nitrogen in model slit pores, using a method developed by us recently [15, 16]. This method allows the permeability of the walls w.r.t the confined fluid to be controlled, while maintaining its atomic nature. Although atomically rough walls have been studied by others as well [17-19], the models used do not allow

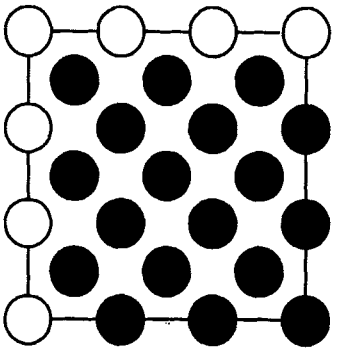

Figure 1 Wall structure in a 108-particle slit pore system at $\rho^* = 0.50$. The length of the box is 6σ with the diameter of each particle corresponding to σ. The open circles are periodic images arising from PBC's.

the permeability of the walls to the confined fluid to be controlled as easily. Our model is quite general and can be used to construct complicated geometries, such as random pore networks, as well.

2 MODEL

The model is based on the conventional NVE method of molecular dynamics for a fluid of N particles in a cube of side L with periodic boundary conditions (PBC's) and the nearest image convention [20]. We used a two-center site-site Lennard-Jones (LJ) shifted potential for nitrogen [21, 22] and a central Lennard-Jones potential for the wall particles of the slit pore. This leads to four LJ interactions between a pair of fluid particles, one LJ interaction between a pair of wall particles, and two LJ interactions between a fluid and a wall particle. The simulations were started with all particles at their FCC lattice sites. To construct the wall of the slit pore, we identify particles that fall on the yz faces of the simulation cube and tether them to their own FCC sites with the tethering potential,

$$\phi_T^*(d^*) = \frac{1}{2}K^* d^{*2} \tag{1}$$

where $d^* = d/\sigma$ is the reduced scalar distance between a tethered particle, and it's tether site (the original FCC lattice position). $K^* \equiv K\sigma^2/\varepsilon$, is a force (spring) constant. ε and σ are the LJ parameters. We have used the simple harmonic potential for this purpose, although others may be used as well. As will be explained in the next section, changing K^* is a very effective means of controlling the permeability of the wall to the confined fluid.

For a 108-particle system, this scheme leads to 18 particles being tethered to the yz face. This is shown schematically in Figure 1. Because of PBC's, this generates automatically an infinite system of walls, infinite in the transverse directions with separation L. For 256 and 500-particle systems, the corresponding number of particles is 32 and 50, respectively. Using this method, a variety of pore shapes can

be constructed easily, by tethering particles at appropriates sites in the basic simulation box. As stated earlier, we chose the wall particles to be all monatomic. In most simulations, for simplicity, the central LJ parameters of the wall particles and the site-site LJ parameters of the fluid particles are assumed to be identical, and equal to the nitrogen site-site parameters ($\varepsilon/k = 37.3$ K, $\sigma = 3.31$ Å, and bond length, $b_e = 1.10$ Å) [21, 22]. This is a one molecule thick model pore wall. Our purpose in this study was to show that the method can be used to vary permeability precisely, and not to model any realistic wall in particular. In a few studies, we did choose the wall parameters (σ, ε, and m) to roughly correspond to those of solid carbon graphite ($\sigma_{wall}/\sigma_{N_2} = 1.03$, $\varepsilon_{wall}/\varepsilon_{N_2} = 0.75$, $m_{wall}/m_{N_2} = 0.43$) [24]. However, we note that this would correspond to a realistic graphite wall only in the limit of large K^* values. It should also be noted, that in view of the preliminary nature of these studies, we have not made any attempt to ensure that the density of the model graphite wall in our studies, corresponds to that of an actual graphite wall. We felt this was unnecessary since our walls in this study are only a molecule thick, which is not the case with actual graphite walls. In the rest of the paper we will refer to these two sets of simulations as model walls (for which the wall and fluid particles have identical molecular parameters) and graphite walls (for which the wall particles have one or more molecular parameters that correspond to graphite), while keeping the above limitations in mind. It should be noted that the tethering potential is active only for the tethered atoms and is in addition to the normal interactions (LJ) between all particles. Details of the simulation technique are given in the Appendix. In the present study, two state conditions were investigated for several values of K^* for model walls, and the results obtained for the diffusion coefficients, wall permeabilities and density and orientation profiles are presented. In addition a few results will also be presented for graphite walls, where we used the usual Lorentz-Berthelot rules for cross interactions. However, all dimensionless variables are still defined using the site-site fluid molecular parameters and are reported as such.

3 RESULTS

3.1 *Diffusion coefficients*

A good measure of the translational freedom of fluid particles in a pore is the diffusion coefficient. In a slit pore there are two distinct diffusion coefficients, one in the direction perpendicular to the pore wall, $D_\perp^*$ (i.e. in the x direction) and the other parallel to the pore walls, $D_\parallel^*$ (i.e. in the y or z directions). In the present simulations, these are obtained from the mean-squared displacement of the fluid particles, measured after the equilibration stage, and for long enough times so that $t \gg L^2/2D$. Thus,

$$D_\perp = \frac{\langle x^2 \rangle}{2t} \tag{2}$$

$$D_\parallel = \frac{\langle y^2 \rangle + \langle z^2 \rangle}{4t} \tag{3}$$

The results obtained at $\rho^* = 0.50$ and $T^* = 2.9$ for model walls are shown in Figure 2, as a function of K^*, the reduced tethering force constant, on a logarithmic

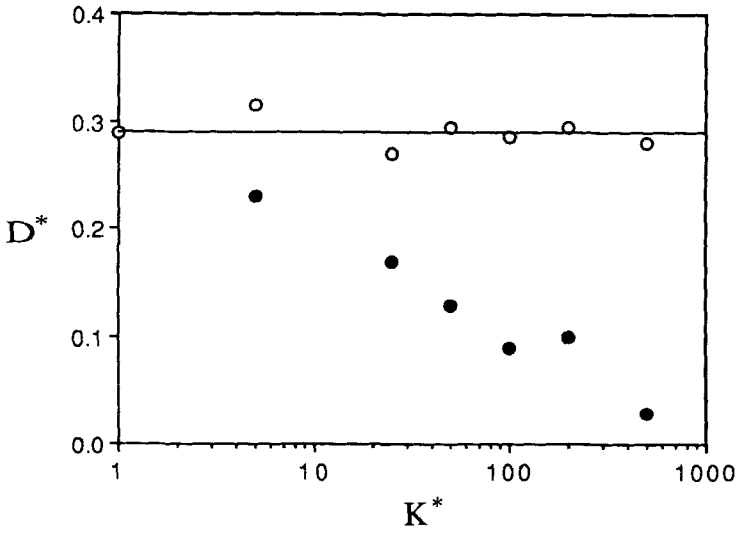

Figure 2 Diffusion coefficients, $D_{\perp}^{*}$ (●), and $D_{\parallel}^{*}$ (○), at $\rho^{*} = 0.50$ and $T^{*} = 2.9$, as a function of K^{*}. The solid line is the diffusion coefficient for the equivalent homogeneous system, consisting of nitrogen molecules only [21].

scale. It shows that at $K^{*} = 5$, $D_{\parallel}^{*}$ and $D_{\perp}^{*}$ are quite similar. As K^{*} increases, $D_{\perp}^{*}$ decreases, whereas $D_{\parallel}^{*}$ is still equal to the homogeneous, bulk fluid value (within statistical accuracy). It follows that the wall becomes more and more impermeable to the fluid as K* increases. This shows that K^{*} is a powerful model parameter for controlling the permeability of the wall. For example, we have a truly "semi-permeable" wall at $K^{*} \approx 30$, where $D_{\perp}^{*}$ has been reduced to approximately half it's original value. At large K^{*} values, the vibrational amplitude is quite small, and the wall particles move very little from their tether sites, thus effectively blocking the fluid from permeating, thereby decreasing $D_{\perp}^{*}$. At low K^{*} values ($K^{*} < 100$), the vibrational amplitude is large and the vibrational frequency is quite small, so there are large enough holes open for long enough times for the fluid particles to go through. This anisotropic behavior of the diffusion coefficient is consistent with experimental observation [23], and is also consistent with results obtained from computer simulation studies of other systems [12]. The insensitivity of $D_{\parallel}^{*}$ to K^{*} is expected, since there is essentially free flow in the y and z directions. In this case only the fluid layer near the walls is effected, and this effect is minimal.

The results obtained for the diffusion coefficients for both model walls and graphite walls are summarized in Table 1, along with other properties. From these results it can be seen that for model walls at the lower density ($\rho^{*} = 0.40$), $D_{\perp}^{*}$ still has an appreciable value at $K^{*} = 500$ (here $D_{\parallel}^{*}$ is higher because of the lower density). Again, at large K^{*} values the wall particles move very little from their tether sites. However, because of the lower density, there are larger permanent holes in the walls, through which some of the fluid particles can still slip through. Thus, no matter how large K^{*} is, $D_{\perp}^{*}$ continues to be appreciable; in this case about 40 percent of the homogeneous value.

Table 1 Summary of results.

Line	ρ^*	L^*	K^*	$\sigma_{wall}/\sigma_{N_2}$	$\varepsilon_{wall}/\varepsilon_{N_2}$	m_{wall}/m_{N_2}	T^{*a}	$D_\perp^{*c}$	$D_\parallel^{*c}$	J_p^*	$\langle U_{px}^* \rangle$
					Model walls						
1	0.50	6.0	500	1.0	1.0	1.0	2.82	0.03	0.280	0.003	0.84
2	0.50	6.0	200	1.0	1.0	1.0	2.90	0.10	0.295	0.012	0.71
3	0.50	6.0	100	1.0	1.0	1.0	2.82	0.09	0.285	0.020	-[b]
4	0.50	6.0	50	1.0	1.0	1.0	2.77	0.13	0.295	0.044	0.54
5	0.50	6.0	25	1.0	1.0	1.0	2.77	0.17	0.270	0.069	-[b]
6	0.50	6.0	5	1.0	1.0	1.0	2.98	0.23	0.315	0.193	0.51
7	0.40	6.463	500	1.0	1.0	1.0	2.91	0.16	0.390	0.013	0.71
8	0.40	6.463	200	1.0	1.0	1.0	2.84	0.15	0.385	0.021	0.61
9	0.40	6.463	25	1.0	1.0	1.0	2.88	0.29	0.390	0.061	0.53
10	0.40	6.463	10	1.0	1.0	1.0	2.72	0.31	0.365	0.091	0.48
					Graphite walls						
11	0.40	6.463	200	1.03	1.0	1.0	2.88	0.16	0.415	0.018	0.61
12	0.40	6.463	200	1.0	0.75	1.0	2.79	0.15	0.390	0.018	0.62
13	0.40	6.463	200	1.03	0.75	0.43	2.78	0.17	0.420	0.013	0.66
14	0.50	6.0	500	1.03	0.75	0.43	2.77	0.02	0.390	0.002	0.91
15	0.60	5.646	500	1.03	0.75	0.43	3.02	0.00	0.140	0.000	na
16	0.60	5.646	500	1.03	0.75	0.43	3.38	0.02	0.130	0.002	0.85

a These are the actual temperatures obtained. The target temperature in all these simulations is 2.9 except in line 16 where it is 3.5 (see Appendix).
b These values have not been calculated.
c The estimated accuracy of $D_\perp^*$ is 15% and that of $D_\parallel^*$ is 10%.

The results for graphite walls are quite similar to those obtained for model walls at the corresponding K^* values and the same state conditions. This is true in all cases, whether the molecular parameters are varied individually (lines 11 and 12) or all are varied simultaneously (lines 13 to 16). Table 1 shows that when the density is increased to 0.60 (line 15), $D_\perp^*$ falls to zero, as would be the case for an actual wall of solid graphite, since it would be completely impermeable. Increasing the temperature at this density from 2.9 to 3.5 (line 16) again increases $D_\perp^*$, mostly because of the increased translational kinetic energy of the nitrogen molecules. $D_\parallel^*$ decreases accordingly when the density is increased.

3.2 *Wall permeabilities*

We also calculated the average 'permeability' of the wall, J_p^*, defined as the number of fluid particles crossing the wall in either direction, per unit time, per unit area. These are also presented in Table 1. J_p^* is related to $D_\perp^*$, the diffusion coefficient perpendicular to the wall, and this relationship will be discussed below.

The effect of K^* on J_p^* for model walls is shown in Figure 3 at $\rho^* = 0.50$ and $T^* = 2.9$. Both J_p^* and $D_\perp^*$ (see Figure 2) decrease with increasing K^*. However, whereas the drop in $D_\perp^*$ when K^* changes from 5 to 25 is relatively small, from 0.23 to 0.17, the drop in J_p^* is quite large from 0.193 to 0.069. This weaker dependence of $D_\perp^*$ on K^* is caused by two effects which cancel each other out. When J_p^* drops from 0.193 to 0.069, rougly one-third as many particles cross the pore wall. This obviously results in a decrease in $D_\perp^*$. On the other hand, the particles that have crossed also find it much harder to return through the pore wall.

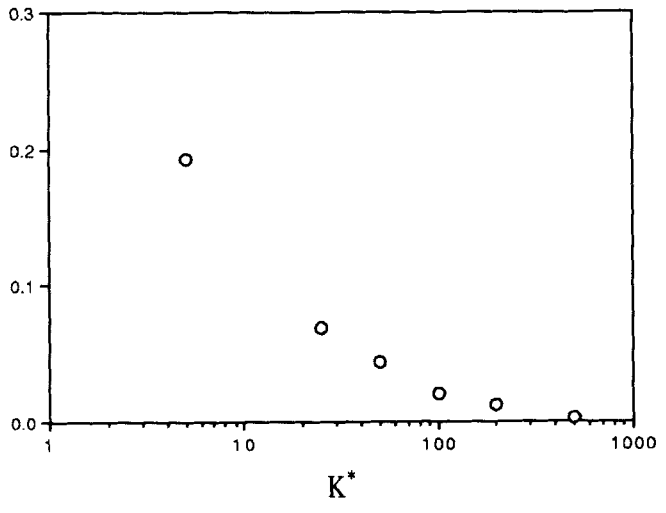

Figure 3 Wall permeabilities at $\rho^* = 0.50$ and $T^* = 2.9$, as a function of K^*.

This effectively increases $D_\perp^*$, cancelling out the decrease to some extent. Similar behavior is observed at $\rho^* = 0.40$ and $T^* = 2.9$ (see Table 1).

The results for J_p^* also show that, at low K^* values (up to about 25) J_p^* increases with density. Again, two opposing effects, the diffusion coefficient and the particle density at the wall surface, explain this behavior. At low K^* values, the decrease in the diffusion coefficient with increasing density is smaller compared to the increase in the number of molecules per unit surface area trying to go through the pore wall. At high K^* values ($K^* > 25$), J_p^* decreases with increasing density. Here, the drop in the diffusion coefficient with increasing density is large enough to more than compensate for the increase in the number of molecules per unit surface area of the wall, thereby decreasing the permeability.

As was the case with the diffusion coefficients, the permeabilities for graphite walls are similar to those obtained for model walls at the corresponding K^* values and state conditions. Again at the higher density of 0.60, J_p^* goes to zero because the smaller holes in the walls and the large K^* values do not let any fluid particles to go through.

3.3 *Density profiles*

The behavior of a fluid in a microporous system is often characterized by the density distribution of the fluid inside the pore. The density profiles for nitrogen in a 108-particle slit pore system are shown in Figure 4 for model walls at several values of K^* at $\rho^* = 0.50$ and $T^* = 2.9$, in the direction perpendicular to the pore wall (i.e. in the x direction). These profiles are center-of-mass density profiles of nitrogen and do not include wall particles. Thus, in the 108-particle slit pore system, we have 90 nitrogen molecules. The profile at $K^* = 500$ corresponds to an almost impermeable wall while that at $K^* = 5$ corresponds to an almost completely permeable wall (as shown in Section 3.1). At the intermediate values, we see the

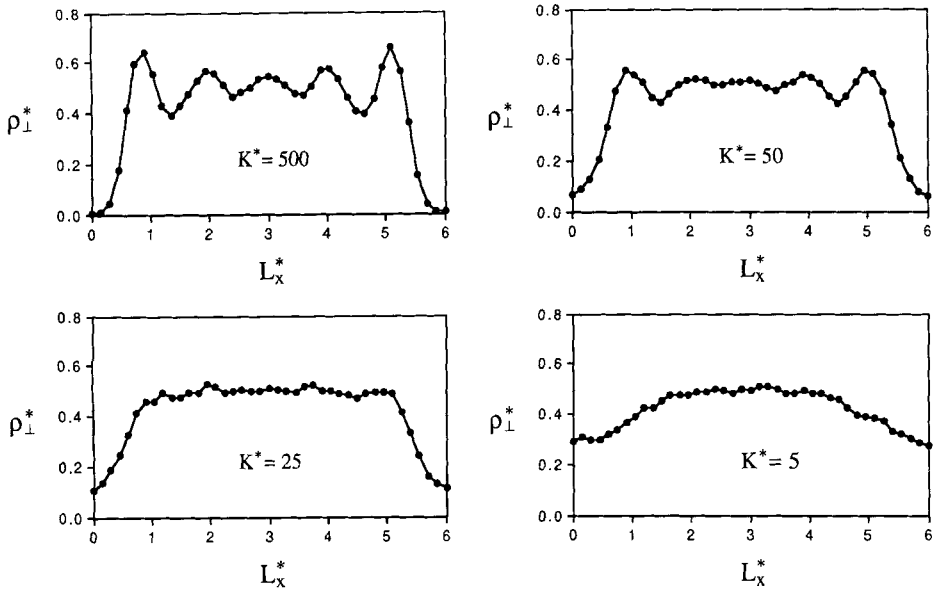

Figure 4 Density profiles of fluid particles perpendicular to the wall at $\rho^* = 0.50$ and $T^* = 2.9$, for several values of K^*. The solid lines are straight line interpolations between the simulation points.

transition from an impermeable to a permeable wall. At $K^* = 5$, $\rho_\perp^*$ does not vary much with position, because the wall is almost totally permeable. At $K^* = 25$, some of the characteristics of impermeable walls can be seen. The density of the fluid at the walls is lower because of the repulsion by the wall. Also, more structure in the density profile is evident. At $K^* = 50$, adsorption and layering can now be clearly seen. This layering effect is well known, especially in it's relationship to adsorption phenomena and leads to adsorption behavior that is observed experimentally [see Reference [24] and references contained therein]. At $K^* = 500$, the density profile is very similar to that obtained from computer simulations and molecular theories for completely impermeable walls by several workers [3, 10, 11, 28]. For these almost impermeable walls, the density of the fluid at the walls is virtually zero. However, we see a distinct peak in the density distribution close to the wall, resulting in part from attraction between the wall and fluid particles. Following this, several other peaks can be seen which get weaker as we get closer to the pore center.

To investigate the effect of system density, we show in Figure 5 the density profile in a similar slit for $K^* = 500$, at $\rho^* = 0.40$ and $T^* = 2.9$. At this lower density, the wall has large enough holes, even at this high K*, to let some of the fluid particles through. This leads to a non-zero density at the walls, unlike for the case when $\rho^* = 0.50$ (see Figure 4). Although not as distinct, we still see an adsorbed layer close to the wall. However, the layering effect is less obvious. The profiles in the directions parallel to the pore walls (i.e. in the y and z directions) are approximately uniform with small amplitude sinusoidal variations. These are also shown in Figure 5. The y and z direction density profiles for the case when $\rho^* = 0.50$, are quite similar to these. The peaks in these profiles correspond to

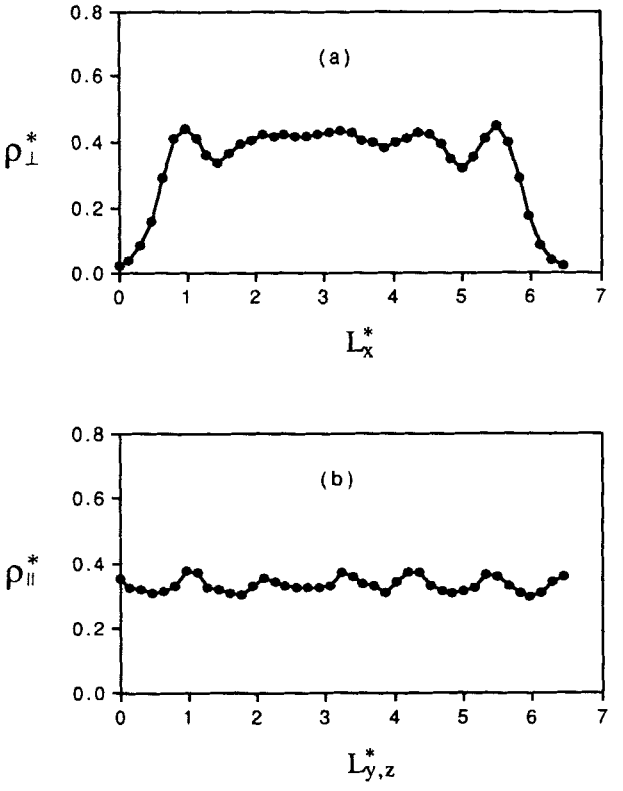

Figure 5 Density profiles of fluid particles perpendicular (a) and parallel (b) to the wall for $K^* = 500$, at $\rho^* = 0.40$ and $T^* = 2.9$.

the holes between tether sites while the valleys correspond to the tether sites. This effect is weak because only the first layer of the fluid particles near the pore wall are effected this way.

The density profiles for graphite walls in all cases are similar to the those obtained for model walls at the corresponding state conditions. However at the higher densities the peaks are somewhat sharper as the fluid particles are packed more tightly at these large K^* values.

3.4 *Orientations*

We also monitored the orientations of the nitrogen particles during the simulation. Table 1 also shows the average orientations of the particles crossing the slit model pore wall in either direction. $\langle U^*_{px} \rangle$ is the average direction cosine along the x axis (i.e. perpendicular to the wall) of all the permeating particles. The results show that at high K^* values the permeating particles have a strong preference to be perpendicular to the wall. This can be seen clearly in Figure 6 which gives the orientation distribution of the permeating particles at $\rho^* = 0.50$ and $T^* = 2.9$, for

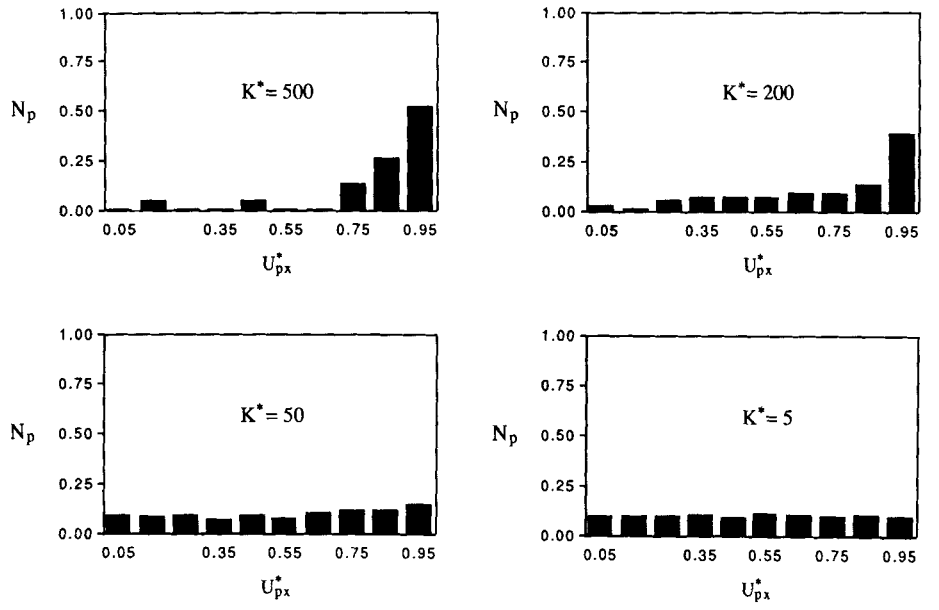

Figure 6 Orientation distributions of permeating fluid particles at $\rho^* = 0.50$ and $T^* = 2.9$, for several values of K^*. N_p is the fraction of permeating particles with orientations in the range $U^*_{px} \pm 0.05$.

different values of K^*. It can be seen that at larger K^* values (e.g. $K^* = 500$) most of these permeating particles are perpendicular to the wall. At large K^* values, the holes in the walls are quite small, so that the fluid particles have to be almost perpendicular to the wall to be able to go through. A few particles do however slip through the wall with orientations other than perpendicular to the wall. At lower values of K^* (e.g. $K^* = 50$ or less), however, the orientation distributions are more uniform, there being large enough holes, for the fluid particles with any orientation to slip through. At intermediate K^* values, the distribution is somewhere between these two extreme cases.

Figure 7 shows the density profiles of nitrogen particles that are either almost parallel or perpendicular to the model pore wall compared with the orientation averaged distributions (also shown in Figure 4), as function of their distance from the pore wall, at $\rho^* = 0.50$ and $T^* = 2.9$. It shows that in the adsorbed layer next to the wall, there are more particles aligned parallel to the wall ($0.0 < U^*_x < 0.2$) than perpendicular to the wall ($0.8 < U^*_x < 1.0$). These parallel orientations are energetically preferred in the adsorbed layer because of its vicinity to the pore wall. This appears to be also true for all the peaks in the density distribution, although such differences are less obvious in the peaks closer to the center. In the valleys between the peaks perpendicular orientations are energetically preferred perhaps because the layers of molecules on both sides are more likely to have parallel orientations. These orientational preferences decrease with decreasing K^* and are almost nonexistent at $K^* = 5$. This general behavior is also observed, although to a lesser extent, at $\rho^* = 0.40$ and $T^* = 2.9$. The above orientational preferences of the fluid particles w.r.t the wall are

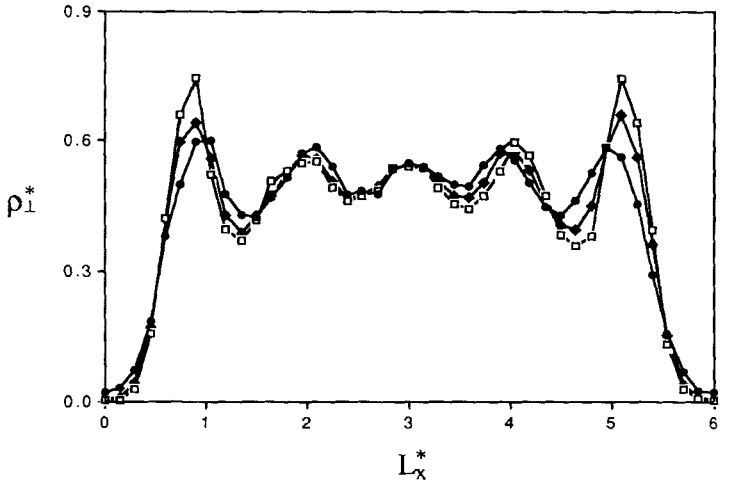

Figure 7 Density profiles ($\rho_\perp^*$) of fluid particles with orientations either perpendicular or parallel to the pore wall at $\rho^* = 0.5$ and $T^* = 2.9$, for $K^* = 500$.
♦ all orientations; □ parallel orientations ($0.0 < U_x^* < 0.2$);
● perpendicular orientations ($0.8 < U_x^* < 1.0$).

in agreement with results obtained by others for similar fluids near a wall [10, 11, 25, 26].

In the case of graphite walls, as can be seen from Table 1, the orientations do not vary significantly from those obtained for model walls.

4 CONCLUSIONS

We have presented results of a molecular dynamics study of nitrogen in model slit micropores using a new method. We showed that the model used for the micropore allows for the permeability of the pore walls to be varied quite simply, by varying the constant in the tethering potential (the permeability can also be varied by varying the LJ parameters of the wall particles), while maintaining the atomic nature of the wall. Anisotropy in diffusion coefficients is observed and the extent of anisotropy depends on the permeability of the confining wall. The density profiles have been shown to have nonuniform behavior and this agrees with experimental observations for impermeable walls. The particles permeating through the wall have been found to have orientations that tend to be perpendicular to the wall at lower permeabilities. Also, it has been shown that the particles in the adsorbed layer next to the walls have orientational preference to be parallel to the wall.

Acknowledgements

This work is supported by the Division of Chemical Sciences, Office of Basic Energy Research, Department of Energy, through Grant No. DE-FG02-87ER13769.

Computing facilities were provided by the University of Illinois Computer Center and Florida State University Computing Center.

APPENDIX: SIMULATION DETAILS

Here we outline the details of the simulation technique employed. All the simulations were carried out on 108 molecules (18 monatomic wall particles and 180 sites for 90 nitrogen molecules). The initial configuration of the system was that of an FCC (see Section 2). The system was equilibrated for about 50,000 time steps and the simulations were run for an additional 200,000 to 300,000 time steps for the properties to converge. We used a reduced time step of 0.0005. The LJ potential was truncated and shifted at 3.0. The translational and rotational equations of motion were solved using Gear's fifth-order predictor-corrector scheme (see Reference [27] for more details on solving the rotational equations of motion). It should be noted that since the tethering force corresponds to an external potential, both the total energy and the total momentum fluctuate around their average values, in contrast to being constant, to within computational errors, in a conventional NVE bulk simulation. Also, since these were NVE simulations, the temperature quoted in the text (2.9 in all simulations, except for line 16 in Table 1 where it is 3.5) is the target temperature, rather than the actual temperature obtained. The actual temperatures obtained are given in Table 1. We found that the mean tethering potential energy $\langle \phi_T(d) \rangle$ for the tethered (wall) atoms was 3/2 $k_B T$ for all K, and indeed each of the Cartesian components of it was 1/2 $k_B T$, as suggested by the equipartition principle.

References

[1] D. Nicholson and N.G. Parsonage, *Computer Simulation and the Statistical Mechanics of Adsorption*, Academic Press, 1982.
[2] A.E. Scheidegger, *The Physics of Flow Through Porous Media*, Macmillan Company, 1957.
[3] Symposium on Molecular Transport in Confined Regions and Membranes, 17th-18th December 1990, Oxford University. Proceedings of this symposium appeared in *J. Chem. Soc. Faraday Trans.*, **87**, 13 (1991).
[4] K.E. Gubbins, "Molecular adsorption in micropores", *Chem. Eng. Prog.*, **86**, 42 (1990).
[5] H.T. Tien, Z. Salamon and A. Ottova, "Lipid bilayer-based sensors and biomolecular electronics", *Crit. Rev. Biomedical Eng.*, **18**, 323 (1991).
[6] J.N. Israelchvili and G.E. Adams, "Measurement of forces between two mica surfaces in aqueous electrolyte solutions in the range 0–100 nm", *J. Chem. Soc. Faraday Trans. I*, **74**, 975 (1978).
[7] J.N. Israelchvili, P.M. McGuiggan and A.M. Homola, "Dynamic properties of molecularly thin liquid films", *Science*, **240**, 189 (1988).
[8] D.D. Awschalom, J. Warnock and M.W. Shafer, "Liquid-film instabilities in confined geometries", *Phys. Rev. Lett.*, **57**, 1607 (1986).
[9] D.D. Awschalom and J. Warnock, "Supercooled liquids and solids in porous glass", *Phys. Rev. B*, **35**, 6779 (1987).
[10] A. Yethiraj and C.K. Hall, "Monte Carlo simulation of hard chain-hard sphere mixtures in slit like pores", *J. Chem. Phys.*, **91**, 4827 (1989).
[11] A. Yethiraj and C.K. Hall, "Monte Carlo simulation of the equilibrium partitioning of chain fluids between a bulk and a pore", *Molec. Phys.*, **73**, 503 (1991).
[12] S.J. Goodbody, K. Watanabe, D. MacGowan, J.P.R.B. Walton and N. Quirke, "Molecular simulation of methane and butane in silicalite", *J. Chem. Soc. Faraday Trans.*, **87**, 1951 (1991).
[13] S.W. Chiu, E. Jakobsson, S. Subramaniam and J.A. McCammon, "Time-correlation analysis of

simulated water motion in flexible and rigid gramicidin channels", *Biophys. J.*, **60**, 273 (1991).
[14] K. Nicklas, J. Bocker, M. Schlenkrich, J. Brickmann and P. Bopp, "Molecular dynamics studies of the interface between a model membrane and an aqueous solution", *Biophys. J.*, **60**, 261 (1991).
[15] J.G. Powles, S. Murad and P. Ravi, "A new model for permeable micropores", *Chem. Phys. Lett.*, **188**, 21 (1992).
[16] S. Murad, P. Ravi and J.G. Powles, "Thermodynamic and transport properties of fluids in permeable micropores", *Fluid Phase Equilibria*, in press (1992).
[17] J.R. Banavar, J. Koplik and J.F. Willemsen, "Molecular dynamics of slow viscous flows", *Computer Simulation Studies in Condensed Matter Physics III*, Springer Proceedings in Physics, Vol. 53, Springer-Verlag, 1990.
[18] G. Mo and F. Rosenberger, "Molecular dynamics simulation of flow in a two-dimensional channel with atomically rough walls", *Phys. Rev. A*, **42**, 4688 (1990).
[19] M.J. Bojan, A.V. Vernov and W.A. Steele, "Simulation studies of adsorption in rough-walled cylindrical pores", *Langmuir*, **8**, 901 (1992).
[20] M.P. Allen and D.J. Tildesley, *Computer Simulation of Liquids*, Clarendon Press, Oxford, 1987.
[21] P.S.Y. Cheung and J.G. Powles, "The properties of liquid nitrogen IV. A computer simulation", *Molec. Phys.*, **30**, 921 (1975).
[22] J.G. Powles and K.E. Gubbins, "The intermolecular potential for nitrogen", *Chem. Phys. Lett.*, **38**, 405 (1976).
[23] J. Caro, M. Bulow, W. Schirmer, J. Karger, W. Heink, H. Pfeifer and S.P. Zdanov, "Microdynamics of methane, ethane and propane in ZSM-5 type zeolites", *J. Chem. Soc. Faraday Trans. I*, **81**, 2541 (1985).
[24] Z. Tan and K.E. Gubbins, "Selective adsorption of simple mixtures in slit pores: A model of methane-ethane mixtures in carbon", *J. Phys. Chem.*, **96**, 845 (1992).
[25] D.E. Sullivan, R. Barker, C.G. Gray, W.B. Streett and K.E. Gubbins, "Structure of a diatomic fluid near a wall. I", *Molec. Phys.*, **44**, 597 (1981).
[26] C. Vega, E.P.A. Paras and P.A. Monson, "Solid-fluid equilibria for hard dumbbells via Monte Carlo simulation", *J. Chem. Phys.*, **96**, 9060 (1992).
[27] S. Murad and K.E. Gubbins, "Molecular dynamics simulation of methane using a singularity-free algorithm", *Computer Modeling of Matter*, P. Lykos, Editor, ACS Symposium Series, **86**, 62 (1978).
[28] J.P.R.B. Walton and N. Quirke, "Capillary Condensation: A Molecular Simulation Study", *Mol. Sim.*, **2**, 361 (1989).